NARROW LINE REGION PROPERTIES

1.1 INTRODUCTION

AGN are very efficient at driving outflows; X-ray and UV spectroscopy reveal high velocity outflows to be nearly ubiquituous on sub-parsec scales in high accretion rate quasars. In recent years, a huge amount of resources have been devoted to searching for observational evidence of galaxy-wide, AGN-driven ouflows, which could provide the feedback mechanism nessecary to quench star formation in massive galaxies. This has resulted in recent detections of winds in AGN-host galaxies using tracers of atomic, molecular, and ionised gas (e.g. Nesvadba et al., 2006; Arav et al., 2008; Nesvadba et al., 2008; Moe et al., 2009; Dunn et al., 2010; Alexander et al., 2010; Harrison et al., 2012; Harrison et al., 2014; Nesvadba et al., 2010; Rupke and Veilleux, 2013; Veilleux et al., 2013; Nardini et al., 2015; Feruglio et al., 2010; Alatalo et al., 2011; Cimatti et al., 2013; Cicone et al., 2014).

One particularly successful technique has been observations of forbiden emission lines, which trace warm (T$\sim 10^4$K) ionised gas in the narrow line region (NLR). Because of its high equivalent width, [O III]λ5008 is most studied of the narrow quasar emission lines. In general, the [O III] emission appears to consist of two components: a narrow, 'core' component, with a velocity close to the systemic redshift of the host galaxy, and a broader 'wing' component, which is normally blueshifted. The general consensus is that the core component traces the gravitational potential of the host galaxy, whereas the wing is tracing outflowing gas.

Observations of broad velocity-widths and asymetries in narrow emission lines stretch back several decades (e.g. Weedman, 1970; Stockton, 1976; Heckman et al., 1981; Veron, 1981; Feldman et al., 1982; Heckman, Miley, and Green, 1984; Vrtilek, 1985; Whittle, 1985; Boroson and Green, 1992). However, the small sample sizes make it difficult to know how representative these observations are. More recently, the advent of large optical spectroscopic surveys (e.g. SDSS) have facilitated studies of the NLR in tens of thousands of AGN (e.g. Boroson, 2005; Greene and Ho, 2005; Zhang et al., 2011; Mullaney et al., 2013; Zakamska and Greene, 2014; Shen and Ho, 2014). This has provided constraints on the prevalence of ionised outflows and, by measuring outflow properties as a function of AGN properties, on the drivers of these outflows. At the same time, there is strong evidence from spatially resolved spectroscopic observations of kinematically disturbed gas extended over galaxy scales (e.g. Greene et al.,

2009; Greene et al., 2011; Hainline et al., 2013; Harrison et al., 2012; Harrison et al., 2014).

However, these studies do not cover the redshift range when star formation and black hole accretion peaked, and consequently when feedback is predicted to be strongest. At these redshifts the bright optical emission lines are redshifted to near-infrared wavelengths, where observations are much more challenging compared to optical wavelengths. As a consequence, studies at high redshifts have typically relied on relatively small numbers of objects, which might not be representative of the properties of the population (e.g. Netzer et al., 2004; Sulentic et al., 2004; Shen, 2016). Other recent studies have looked at the [O III] emission properties of rare sub-samples - e.g. heavily obscured quasars (Zakamska et al., 2016) and the most luminous quasars (Bischetti et al., 2016). These studies often report exceptionally large [O III] widths, with FWHM $> 1000 \mathrm{km\,s^{-1}}$(e.g. Netzer et al., 2004; Nesvadba et al., 2008; Kim et al., 2013; Brusa et al., 2015; Carniani et al., 2015; Perna et al., 2015; Bischetti et al., 2016). This could suggests that AGN efficiency in driving galaxy-wide outflows increases with AGN luminosity. In addition, [O III] is often very weak, or is missing entirely (e.g. Netzer et al., 2004).

In this chapter we analyse the [O III] properties of a sample of 356 high-luminosity, redshift $1.5 < z < 4$ quasars. The large sample size will help to put these observations in context of the AGN population as a whole. We will analyse the [O III] emission properties as a function of key properties of the quasar, e.g. BH mass, luminosity, and accretion rate.

1.2 QUASAR SAMPLE

We have assembled a catalogue of 356 high-luminosity, redshift $1.5 < z < 4$ quasars. These are selected from our near-infrared spectroscopic databse (Chapter 2) to have spectra covering the strong, narrow [O III] doublet. The broad Balmer Hβ line is also observed for all but two of the sample. In 165 the spectra extend to the broad Hα emission at 6565Å, and in 260 optical spectra including C IV are also available (mostly from SDSS/BOSS). This is the largest study of the narrow line region properties of high-z quasars ever undertaken. The quasar sample is summarised in Table 1.1.

1.3 PARAMETERIC MODEL FITS

In this section we describe how parameters of the [O III] emission are derived. Our approach is to first model the spectra, and then derive parameters of interest from the best-fitting model. This enhances the useful information that can be extracted from spectra with finite signal-to-noise (S/N).

Table 1.1: The numbers of quasars with [O III] line measurements and the spectrographs and telescopes used to obtain the near-infrared spectra.

Spectrograph	Telescope	Number
FIRE	MAGELLAN	31
GNIRS	GEMINI-N	28
ISAAC	VLT	9
LIRIS	WHT	7
NIRI	GEMINI-N	29
NIRSPEC	Keck II	3
SINFONI	VLT	80
SOFI	NTT	76
TRIPLESPEC	ARC-3.5m	27
TRIPLESPEC	P200	45
XSHOOTER	VLT	21
		356

Two independent and complementary models are considered. The first consists of a power-law continuum, an empirical Fe II template and multiple Gaussian components to model the emission from the broad and narrow components of Hβ and the [O III] doublet. This is a model which is commonly adopted in the literature. The second model consists of six spectral components derived from an independent component analysis (ICA) of a large sample of low-redshift AGN with SDSS spectra covering the same spectral region. As we will demonstrate, a linear combination of these spectral components is able to reproduce the spectra around Hβ/[O III] to a high degree of precision.

1.3.1 *Model One: Multiple Gaussians*

The first step of our procedure is to fit a combination of a power-law continuum and an optical Fe II template – taken from Boroson and Green, (1992) – to two windows at 4435-4700 and 5100-5535 Å. This requires the spectra to be transformed to the quasar rest-frame. The redshift used in this transformation is either derived from the peak of the broad Hα emission ($\sim$ 40 per cent of our sample), from the peak of the broad Hβ emission ($\sim$ 40 per cent) or from the peak of the narrow [O III] emission (20 per cent). In later sections, the quasar systemic redshift will be refined using, for example, our model fits to the [O III] emission. At this stage however, sucessfully implementing our fitting procedure only requires the quasar rest-frame to be determined to within a few 1000km s^{-1}. The Fe II template is convolved

with a Gaussian, and the width of this Gaussian, along with the normalisation and velocity offset of the Fe II template, are free variables in the pseudo-continuum fit.

The following model is then fit to the spectra in the wavelength interval 4700-5100 Å. The fit is done as a function of the Doppler velocity shift, and we adopt the wavelength 4862.721Å (the laboratory Hβ wavelength) to transform wavelengths into equivalent Doppler velocities. In general, Hβ is modelled by two Gaussians with non-negative amplitudes and FWHM greater than 1200km s^{-1}. In 10 objects Hβ is modelled with a single Gaussian. In 41 Hβ is modelled with two Gaussians, but the velocity centroids of the two components are constrained to be equal. This is normally because the spectrum is low S/N, and adding extra freedom to the model does not significantly decrease the minimised reduced chi-squared. In addition there are cases where the blue wing is below the lower wavelength limit of the spectrograph; employing a symmetric model then allows us to model with spectrum with reduced constraints.

Contributions to the Hβ emission from the narrow-line region is weak in the vast majority of our sample, and in general we do not include an additional Gaussian component to model this emission. In 9 objects features in the model - data residuals suggest that a narrow emission component is significant, and an additional narrow Gaussian is included for these quasars. It is likely that there is some not insignificant contribution from the narrow line region in other quasars. If this is the case then measures of the Hβ velocity width will be biased to lower values on average. However, in this chapter we are only interested in measuring the peak of the Hβ emission (to infer the quasar redshift). This is unlikely to be biased by not decomposing the narrow and broad emission components.

Each component of the [O III] doublet is fit with one or two Gaussians, depending on the fractional reduced χ^2 difference between the one- and two-component models. If the addition of the second Gaussian decreases the reduced χ^2 by more than 5 per cent then the double-Gaussian model is accepted. One hundred and thirty-one are fit with a single Gaussian and 154 with two Gaussians. In a further 71 objects [O III] is very weak or the spectrum is very low S/N. In these quasars we vary the normalisation of a fixed [O III] template (see below). When a single Gaussian is used to model each line, the peak flux ratio of the [O III] 4960 Å and 5008Å components are fixed at the expected 1:3 ratio and the width and velocity offsets are set to be equal. In the double Gaussian fit, the peak flux ratio of the second components is again fixed at 1:3, and the width and velocity offsets are again set to be equal.

In many objects [O III] is undetected, or is very low S/N. In these cases we do not attempt to measure the width of the [O III] emission, but instead fit a fixed [O III] template, in order to measure the EQW.

The template is derived by running our fitting routine on a very high S/N composite spectra of low redshift AGN.

1.3.2 *Derived parameters*

All [O III] line properties are derived from the [O III]5008 emission, but, as described below, the kinematics of the peak at 4960Å are constrained by our fitting routine to be identical.

We do not to attach any physical meaning to the individual Gaussian components used in the model. While it is true that in some quasars the [O III] emission can be clearly separated in to a narrow component at the systemic redshift and a lower-amplitude, blueshifted broad component (e.g. Shen, 2016), often this decomposition is highly uncertain. Furthermore, often the S/N is not sufficient to statistically justify the addition of a second Gaussian component. It is artifical to decompose the [O III] profile in to core and wing using two Gaussians. No theoretical justification that the wing compoent should have a Gaussian profile. And decomposition depends on S/N, spectral resolution. Instead we use non-parameteric measures from the whole profile.

Instead, we characterize the [O III] line profile using a number of non-parameteric measures, which are commonly used in the literature (e.g. Zakamska and Greene, 2014; Zakamska et al., 2016). A normalised cumulative velocity distibution is constructed from the best-fitting model, from which the velocities below which 5, 10, 25, 50, 75, 90, and 95 per cent of the total flux accumulates can be read off. The width of the emission line can then be defined, for example, using $w_{80} = v_{90} - v_{10}$. The absolute assymetry in the line profile A is defined as $((v_{95} - v_{50}) - (v_{50} - v_5))/(v_{95} - v_5)$ (Zakamska and Greene, 2014).

We also define the blueshift of the [O III] emission, which is a measure of the velocity shift of the profile from the expected position. This requires a measure of the observed line position, and an accurate measurement of the quasar systemic redshift. We use v_{10} to mesaure the location of the [O III] emission. We use the peak of the full [O III] profile to define the systemic redshift, and verify below that this is unbiased.

The line width measures are not at present corrected for instrumental broadening, but this can easily be done.

1.3.3 *Reliability of derived parameters*

Removal of Fe II emission

As highlighted by Netzer et al., (2004), there is a prominent Fe II emission feature just redward of [O III]λ5007. Accurately modelling and
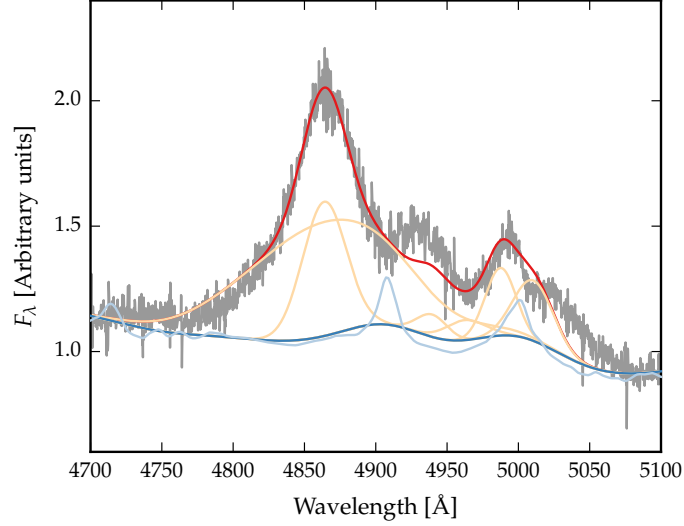
Figure 1.1: Example where poorly subtracting the iron can be confused with [O III].

subtracting this emission is important, because failure to do so will lead to large errors in the inferred [O III] line parameters. However, the relative strengths of the Fe II lines can differ significantly from those of I Zw 1 on which the Fe II template is based.

An example of this is shown in Fig. 1.2. This object was studied by Shen, (2016), but residual Fe II was mistakenly identified as [O III], resulting in a catastrophically wrong systemic redshift estimate. Fitting the power-law+Fe II subtracted spectrum with the Gaussian model leads to a very broad and redshifted total [O III] emission profile. It's difficult to definitely rule out the origin of the emission as very broad and redshifted [O III] emission, but a much more likely scenario is that this is excess Fe II emission which is poorly modelled by the empirical template that we employ. In a later section we demonstrate how this spectrum can be extremely well fit by the ICA components with very little contribution from [O III].

We estimate that this has a significant effect in 58 quasars in our sample. The majority of these (41) are flagged as having low EQW [O III]. This is expected from the well-known anti-correlation between the strengths of Fe II and [O III] (Eigenvector 1). Therefore, our failure to adequtely remove the Fe II emission does not really affect our ability to measure the [O III] properties. The biggest problem is if residual Fe II emission is misidentified as [O III] (e.g. Netzer et al., 2004).

In 3 objects, there is a plateau-like emission. It's difficult to know what fraction of this emission is Fe II, and what fraction is [O III].

This doesn't mean we are having to exclude all of these because of the Fe II - [O III] is missing in most anyway.
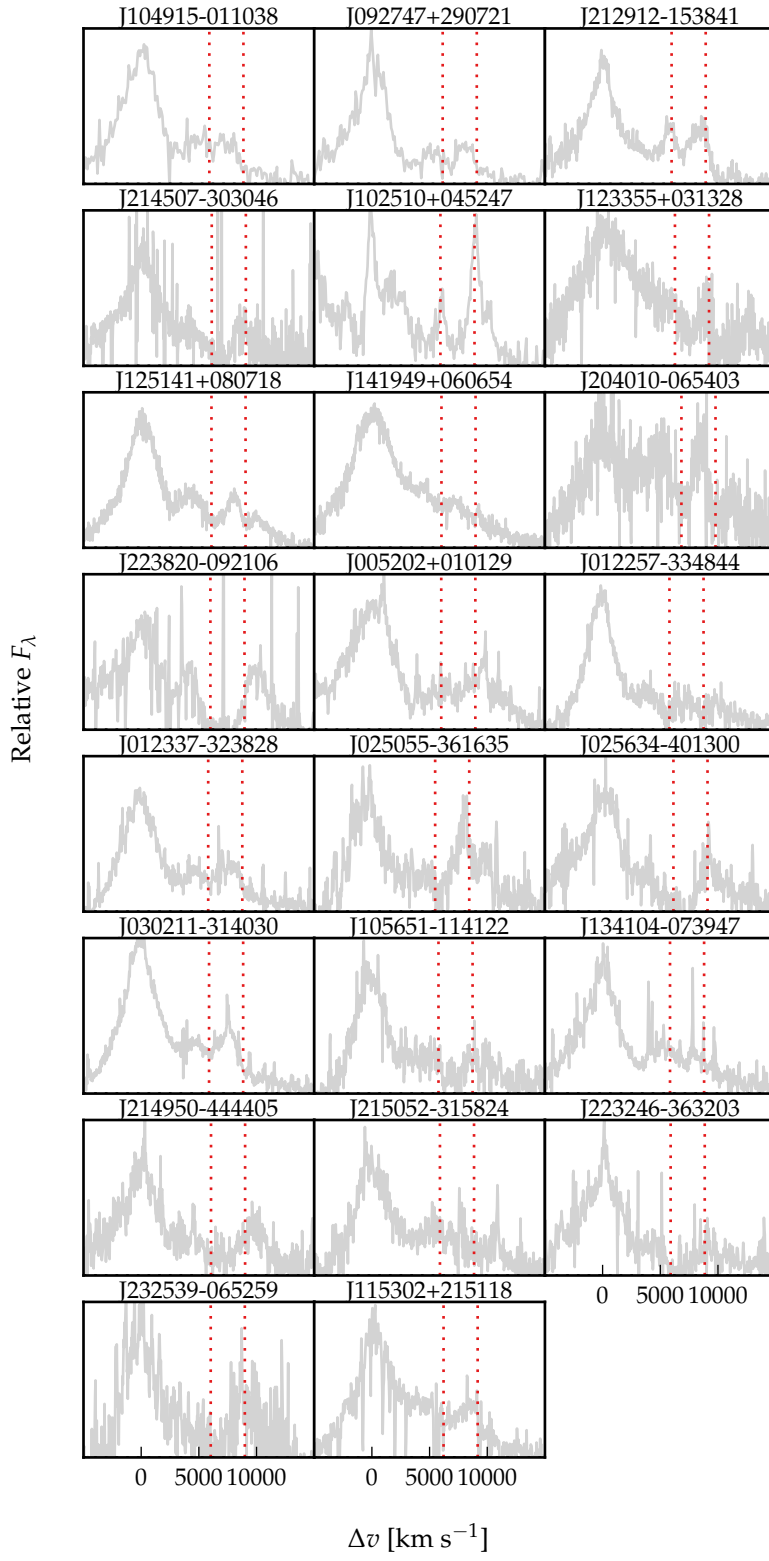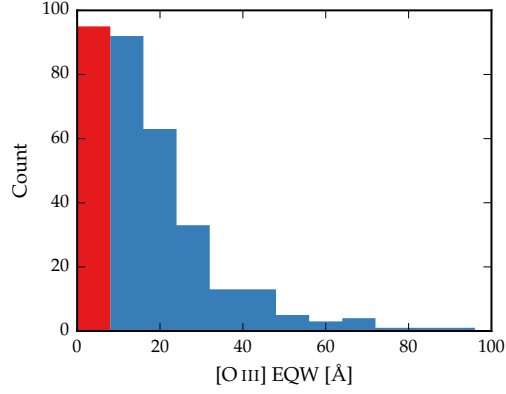
Figure 1.2

Figure 1.3: Anything to the left of the line [O III] is too weak to derive paramters from Gaussian fits. Excludes 120 objects.

Low EQW [O III]

If the EQW is too low then the shape of the [O III] emission cannot be measured reliably, regardless of the S/N of the spectra. We therefore impose an EQW cut of 8Å on our derived parameters.

Note that if very low EQW or S/N I fit with fixed model just to get an estimate of the EQW.

Low S/N [O III]

1.3.4 *Extreme [O III]*

Model parameters were derived using a standard variance-weighted least-squares minimisation procedure employing the Levenberg-Marquardt algorithm. Prior to the fit, the spectra were inspected visually and regions significantly affected by telluric absorption or of low S/N were masked out.

1.3.5 *Approach Two: Independent Component Analysis*

Independent component analysis (ICA) is a blind source separatation tecnique for separating a signal in to linearly mixed statistically independent subcomponents. Unlike the more widely-used principle component ananlysis technique, ICA produces non-negative components which allows for a physical interpretation of the components and weights. ICA has been succesfully applied to model the spectra of emission-line galaxies (Allen et al., 2013) and BAL quasars (Allen et al., 2011). The quasar spectra can be thought of as a set of observa-
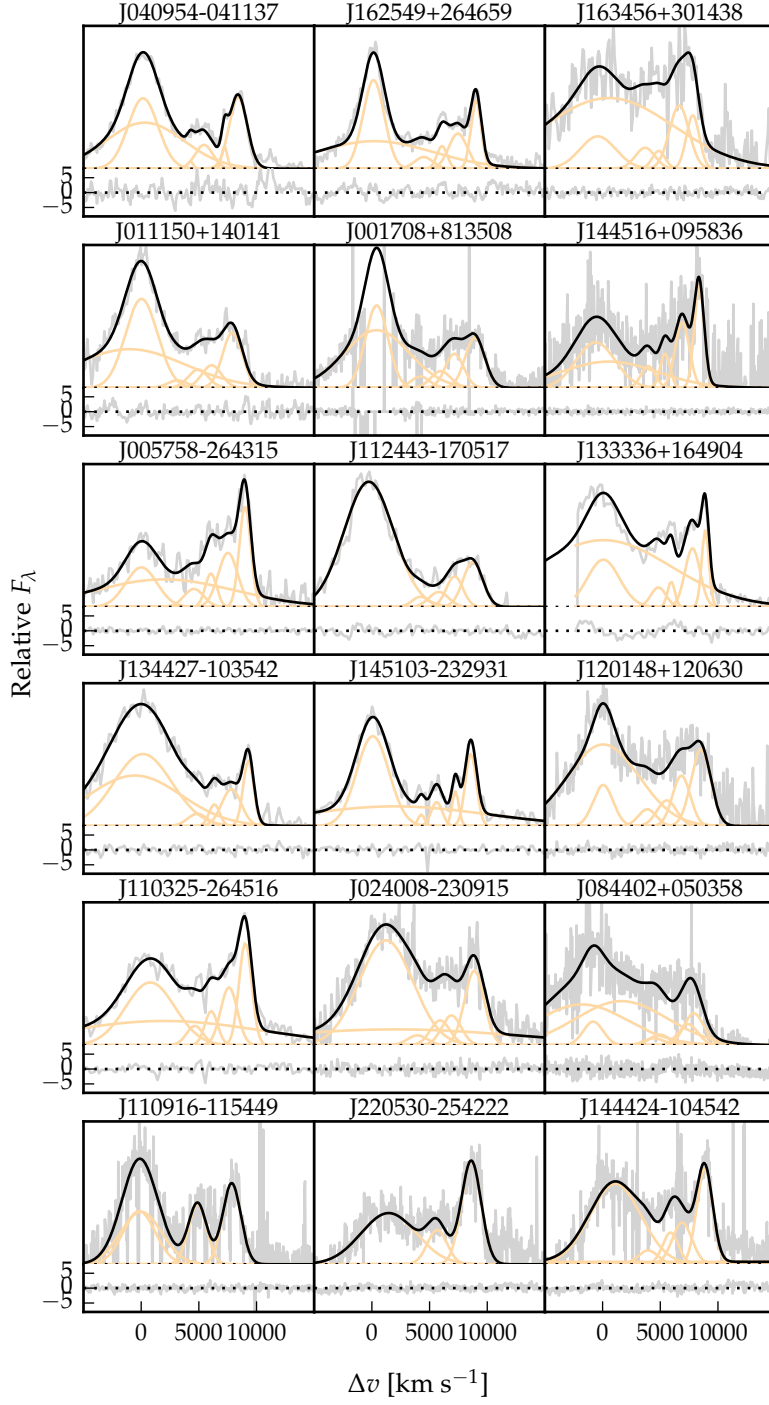
8

Figure 1.4: Extreme [O III] emission profiles.

tions, x, which are made up of statistically independent components, c, that are combined by some mixing matric, W:

$$x = Wc \qquad (1.1)$$

ICA reverses this proces and describes how the observed data are generated. Both the independent components and the mixing matrix are unknown, but can be gound by solving:

$$c = W^{-1}x. \qquad (1.2)$$

The components were solved for using a sample of 2,154 SDSS quasars at redshifts XX. At these redshifts the SDSS spectrograph covers the rest-frame region XX-XXÅwhere Hβ and [O III] lie. The individual spectra were first adjusted to give the same overall shape as a model quasar template spectrum. Six positive independent components and four additional components that could be negative were found to be sufficient to reconstruct the spectrum, without over-fitting. Each quasar spectrum can then be represented as a linear combination of the independent components:

$$x_j = \sum_{i=1}^{10} c_{ij} W_{ij} \qquad (1.3)$$

For each quasar in our NIR sample perform a variance-weighted least-squares minimisation to determine the optimum value of the components weights. A power-law was fit to the quasar template spectrum in emission line free windows at 4200-4230, 4435-4700 and 5100-5535 Å. Each of the components is then divided by the power-law. An identical process is performed on each of the spectrum to be fitted, so that there is essentially zero shape in both the components and the spectrum to be fitted.

We do a preliminary fit. First six components constrained to have positive weights. Good fits were achieved for 334 out of the 358 spectra. Fit is done in log-wavelength.

An example is shown in Fig. 1.5.

Although the ICA is analysis is not based on any physics, there appears to be a direct correspondence between the individual components and the different emission features which contribute to the spectra (Fig. 1.5). This correspondence is summarised in Table 1.2. The component w_1 seems to correspond to Fe II emission, the components w_2 and w_3 to broad Hβ emission, the components w_4 and w_5 to narrow [O III] emission at the systemic redshift, and the component w_6 to broad, blueshifted [O III] emission.
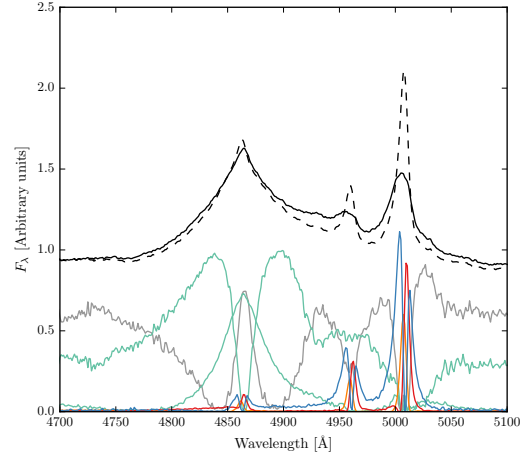
Figure 1.5: Black solid line is the median from the ICA fits to the high-luminosity sample. Black dashed line shows the median from the low-luminosity sample. The six positive ICA components are also shown.

Table 1.2: Approximate physical origin of the ICA components.

Component	Origin
w_1	Fe II
w_2	Hβ
w_3	Hβ
w_4	[O III] core
w_5	[O III] core
w_6	[O III] wing
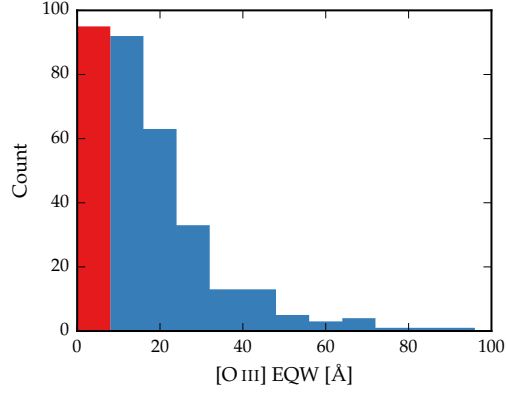
Figure 1.6: Anything to the left of the line [O III] is too weak to derive paramters from Gaussian fits. Excludes 148 objects.

1.3.6 *Bad ICA fits*

There are 24 cases where the the ICA components are unable to reproduce the quasar spectrum. These are normally when we have very broad [O III]. These are clearly lacking in any significant number in the low redshift sample used to generate the ICA components.

1.3.7 *Reconstructing the [O III] profile*

We take our best fitting ICA component weights, and set the first three to zero. We define the boundaries of [O III]λ5008 as being between 4900 and 5500Å. The blue wing of [O III]λ5008 is blended, and so to recover the intrinsic profile we instead use the blue wing of [O III]λ4960.

Doesn't this need to be scaled?

Defining a sample for Gaussian fits

In this section we define a sample of objects for which we believe the emission line properties we infer to be reliable. Specifically, the velocity measures such as w_{80}.

First of all we flag objects where the [O III] emission is too weak. To do this we look at the distribution of power which is in the [O III] weights. This is shown in Figure 1.6. We exclude all objects where the [O III] strength is less than 0.1165. This corresponds to an equivalent width of XX.

We use the ICA components to generate high S/N representations of the spectra. We take the error spectrum from the object, and scale it so that the S/N (which is measured in the continuum and is quoted per pixel) is {2.5, 5, 7.5, 10, 15, 20, 50}. We interpolate the ICA model flux on to the wavelength of the object. For each S/N, we run our
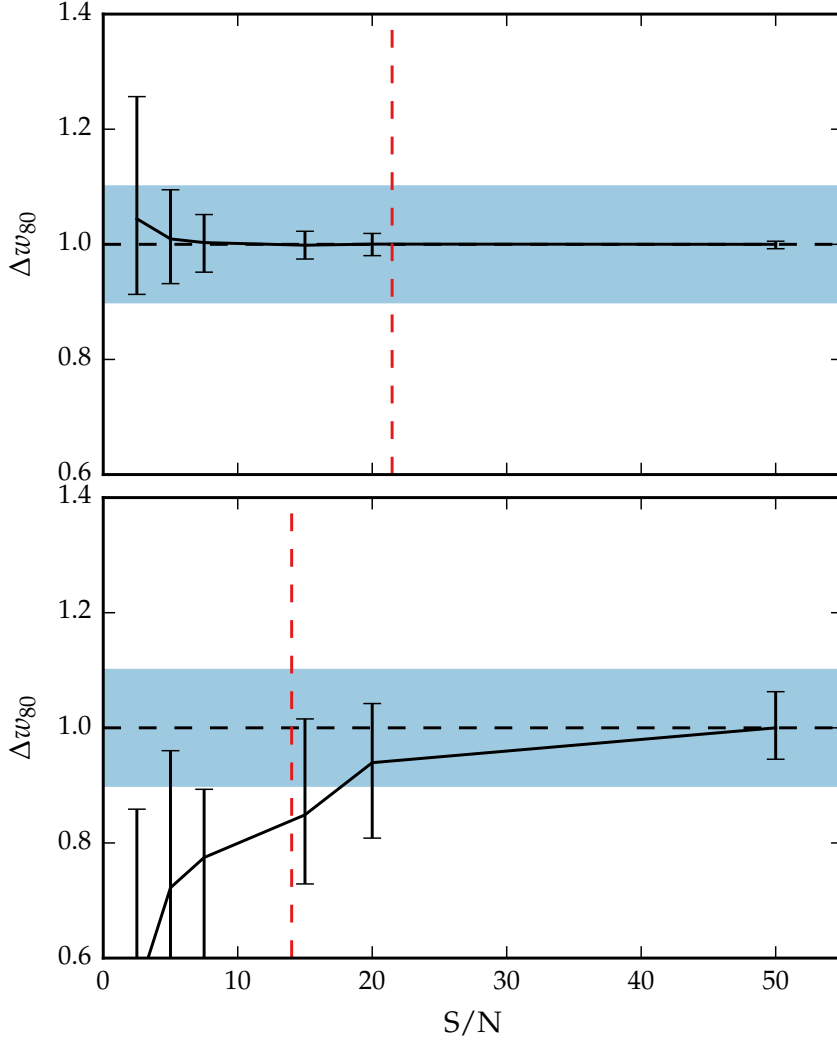
Figure 1.7

line-fitting procedure 500 times. In each of the 500 trials the flux is drawn randomly from a Normal distribution with $(\mu = F_\lambda, \sigma = \sigma_\lambda)$.

In the next step, we calculate the 16th, 50th and 84th percentiles of the distribution of w_{80} values. This is shown in Figure 1.7, where the marker denotes the 50th percentile, and the lower and upper error bars the 16th and 84th percentiles respectively. As expected, the uncertainty on w_{80} increases as the S/N of the spectrum decreases. The true value of w_{80} is defined as being the value in the highest S/N reliation of the spectrum (S/N=50). If the fractional change in w_{80} at the actual S/N of the spectrum is greater than 10 per cent, or the error in w_{80} is greater than 50 per cent, then the measurements are flagged as being unreliable.

We also exclude the 24 objects where the ICA fits failed, because we can't perform the S/N test for these objects.

We exclude the objects for which the ICA fit failed to reproduce the spectrum (24 objects). If the emission is too

Looked at distribution of OIII strength. Excluded objects below cut. Then also exclude S/N based on simulations Reconstruct high S/N spectrum using MFICA components Then degrade S/N: Take typical noise spectrum for each instrument and add a scaled version of this. Simulate 500 trials for each S/N level. Take median and 68% as the measurement and its error

1.3.8 *Derived Parameters*

1.3.9 *Other flags*

Flag 2

Low S/N. Includes some of the strong iron emitters.

Flag 3

74 objects where [O III] is undetected, although I don't have a rigorous definition of what this means. Merge with 2? Section on deriving upper limits.

1.4 ICA COMPONENT FITS

What is the segue here? Sometimes Gaussians give poor fit? Not clear what is Hb, what is OIII, what is Fe? Show some examples of when the multi-Gaussian fits fail. Need to describe sample used in ICA component decomposition and briefly describe method (or refer to Allen & Hewett).

1.5 MEASURING THE QUASAR SYSTEMIC REDSHIFT

Explain flags Need to send paul redshifts

1.5.1 *Hα*

There are 224 quasars in our sample with spectra covering the Hα emission line. We discard seven of these from our sample because of very low S/N (<2.5 measured in the Hα line), leaving 217 To measure the position of the line we fit a parameteric model, which is very similar to the model described in Paper I. The continuum emission is first modeled and subtracted using the procedure described in Paper I. We then test five different models with increasing degrees of freedom to model the Hα emission. The model we select is the simplest model for which the fractional change in the reduced chi-squared

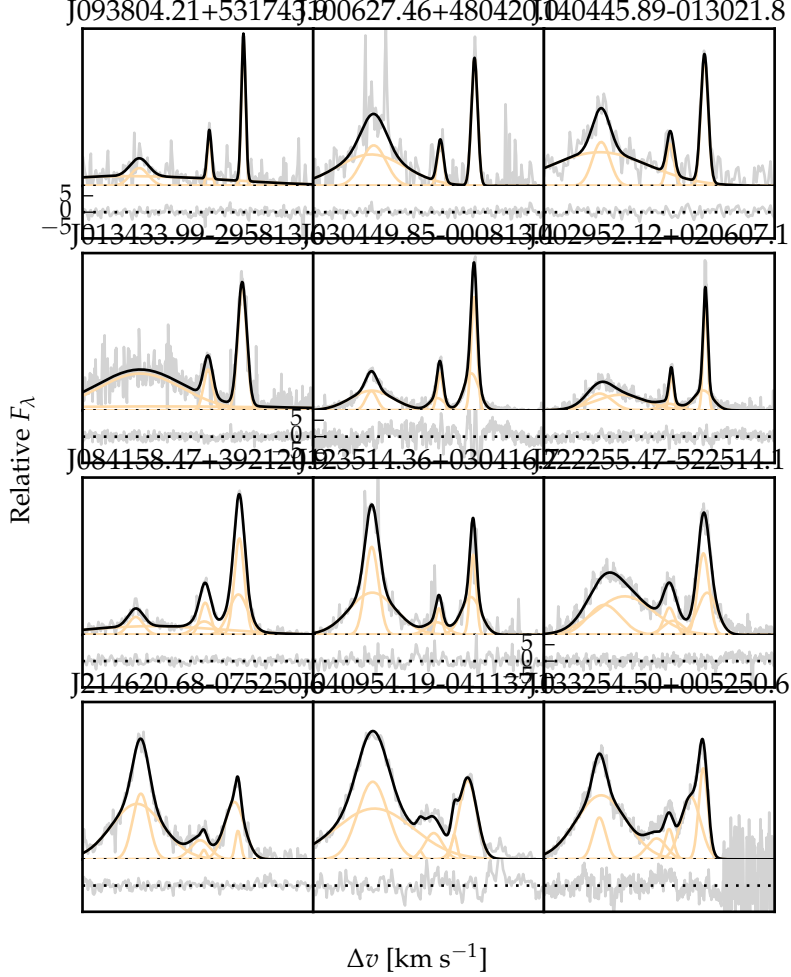Figure 1.8: Multi-component Gaussian fits to the continuum-subtracted Hβ/[O III] emission in 16 quasars, chosen to be the representative of the wide range of [O III] line widths we measure in our sample. The data is shown in grey, the best-fitting parametric model in black, and the individual model components in orange. The broad Hβ centroid is used to measure the systemic redshift, and Δv is the velocity shift from the line rest-frame transition wavelength for Hβ. Below each fit we plot the data minus model residuals, scaled by the errors on the fluxes. **Resample model at higher resolution.**
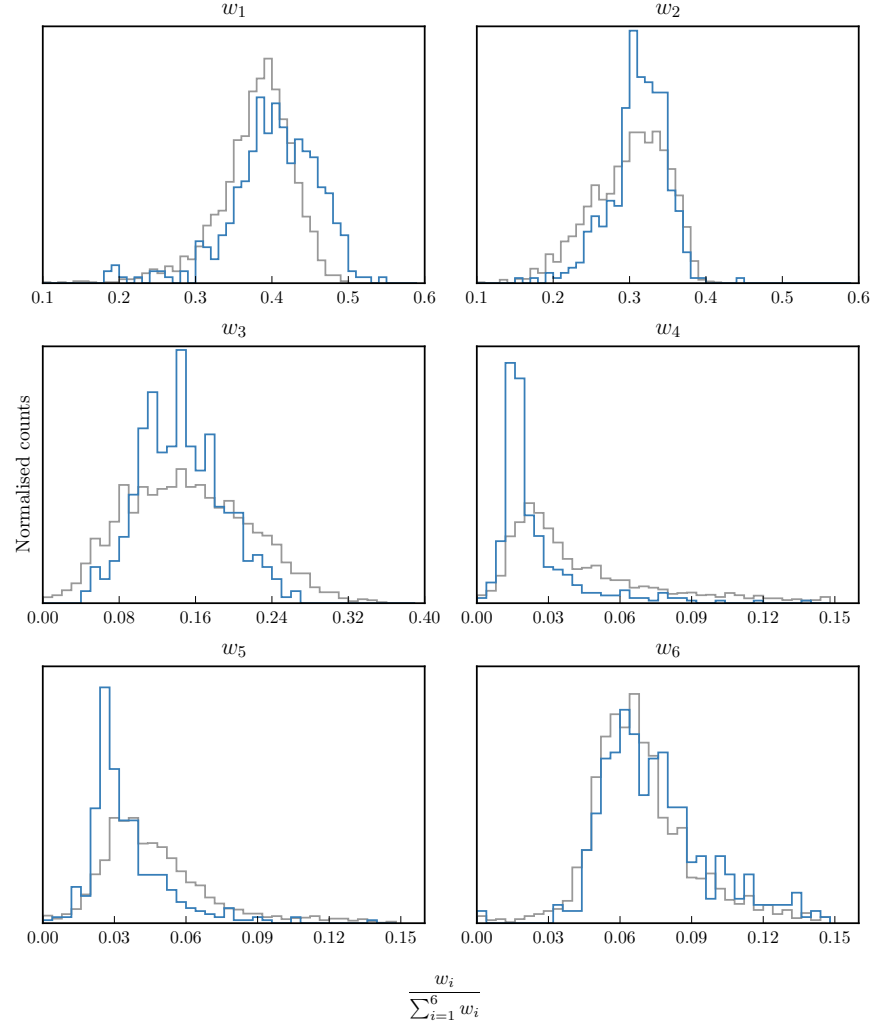
Figure 1.9: The relative weight in each of the six positive ICA components for the high-luminosity (blue) and low luminosity samples (grey). In the high-luminosity sample Fe II emission is stronger (component w_1). The core [O III] emission is weaker (components w_4, w_5) but the strength of the blueshifted wing is the same (w_6).

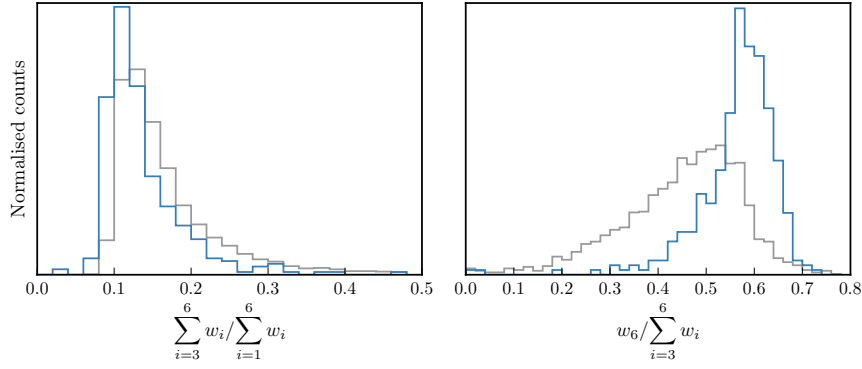Figure 1.10: The relative weight in the three ICA components correspond-
ing to [O III] emission (*left*) and the relative weight of the com-
ponent most closely related to blueshifted [O III] emission rel-
ative to all three [O III] components (*right*). [O III] emission is
weaker in the high-luminosity sample, but the relative contri-
bution but the fractional contribution from the blueshifted com-
ponent to the total [O III] emission is higher. Hence [O III] is
weaker, broader, and more asymmetric in the high-luminosity
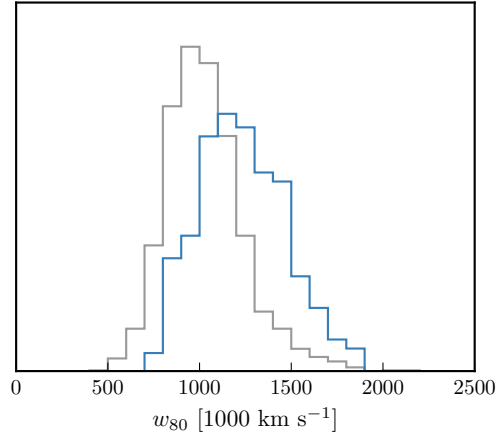sample. See Zakamska discussion.

Figure 1.11: Comparison of [O III] velocity-widths in the high and low lumi-
nosity samples using the ICA component fits. If keep this need
to explain in text how w_{80} is calculated from ICA component
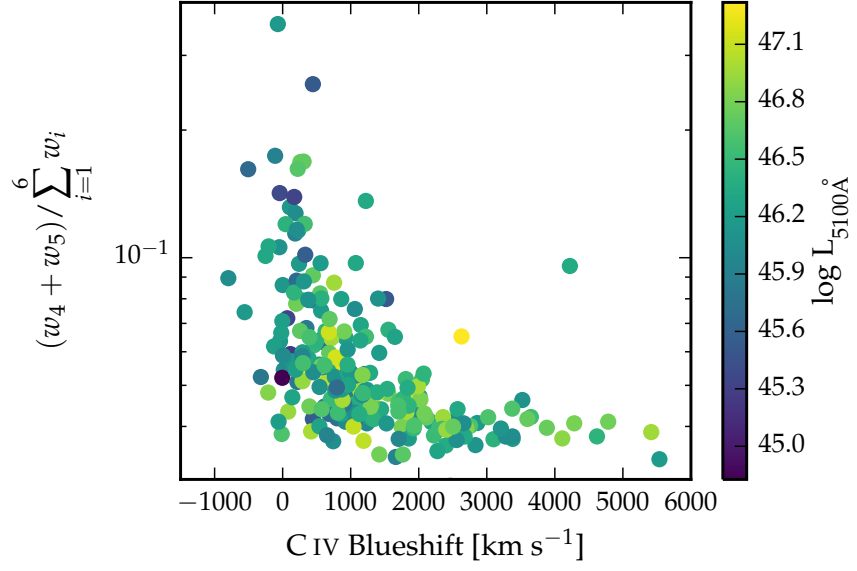fits.

Figure 1.12: [O III] strength decreases as the C IV blueshift increases, I run in to problems comparing the C IV blueshift to the [O III] blueshift / velocity-width. See similar thing if I use [O III] EQW instead. Need to fix y ticks. Only showing the core components here. The C IV blueshift is now measured relative to the NIR ICA redshift. I think this is trend is mostly being driven by the Eigenvector 1 correlations: as the blueshift increases the Fe II strength increases and the [O III] strength decreases. Doesn't appear to be driven by the luminositiy. Is this tighter than EV1 trend shown with Fe/OIII strength by other authors? Is the AGN NLR absent in objects where outflows have reached kiloparsec scales, sweeping up the low-density material responsible for the [OIII]-emission?
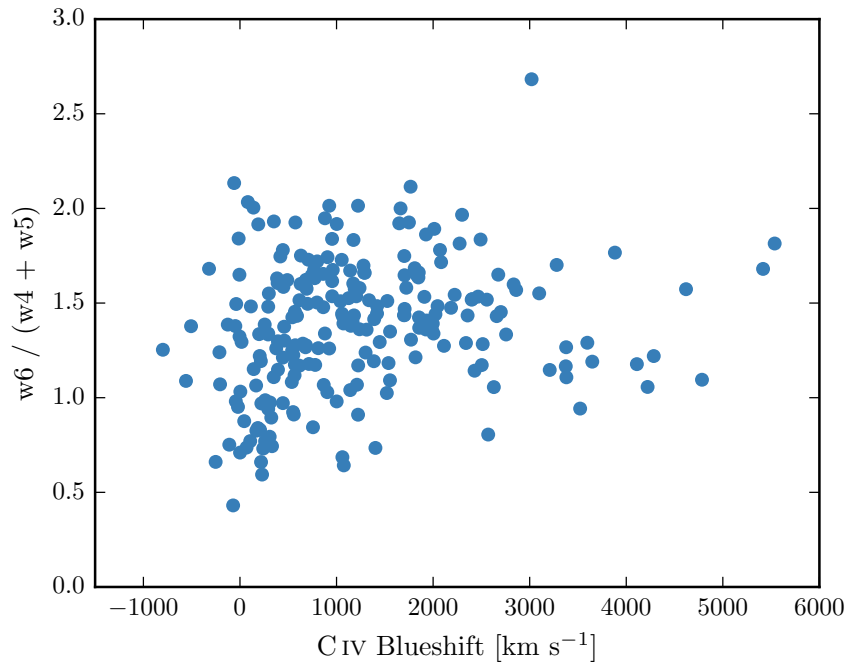
Figure 1.13: I think there is a trend here but at high blueshifts the OIII is undetected / very low S/N. Need to determin when we can believe OIII paramters. Why at low CIV blueshift is there a much bigger dynamic range than in [O III] blueshifts in Fig. 13. Is it just because we have more objects?
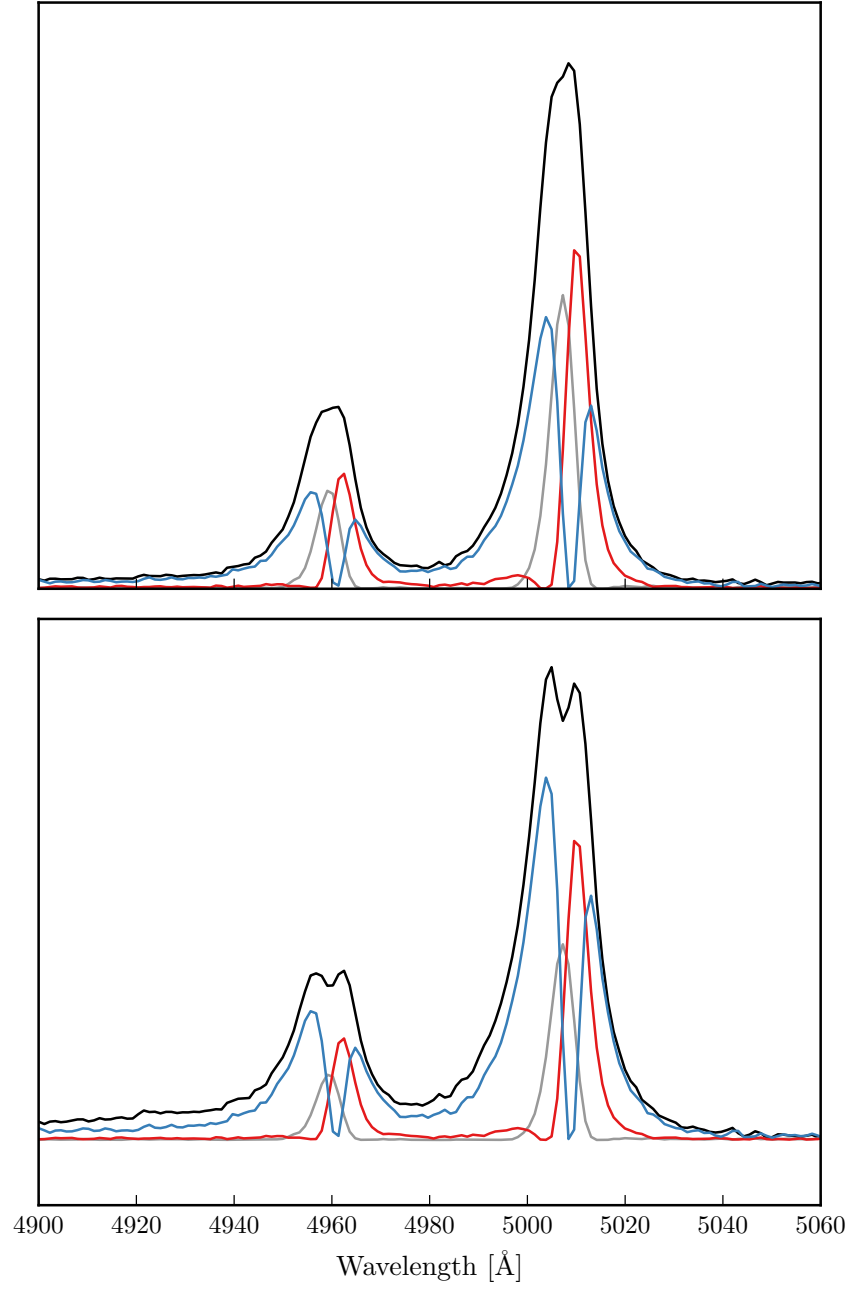
Figure 1.14: Comparison of median [O III] profiles from ICA fits it low- and high-luminosity samples.
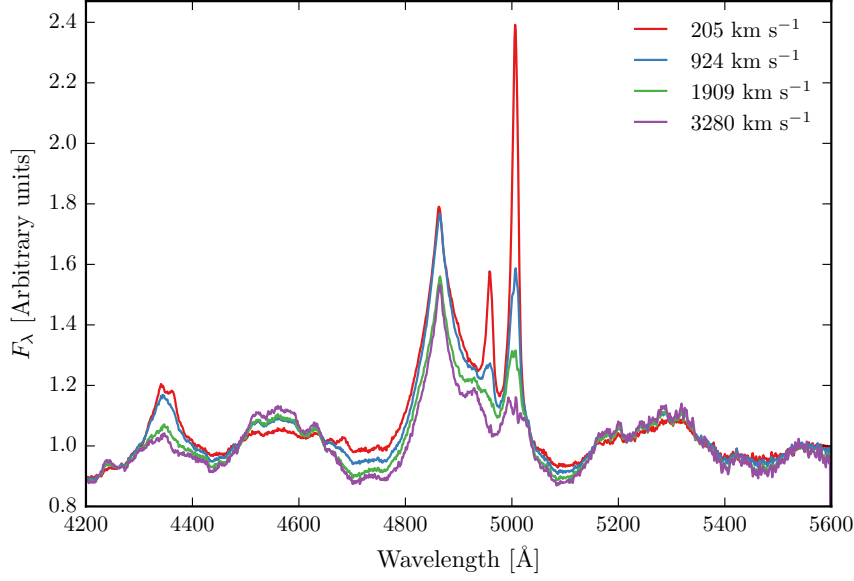
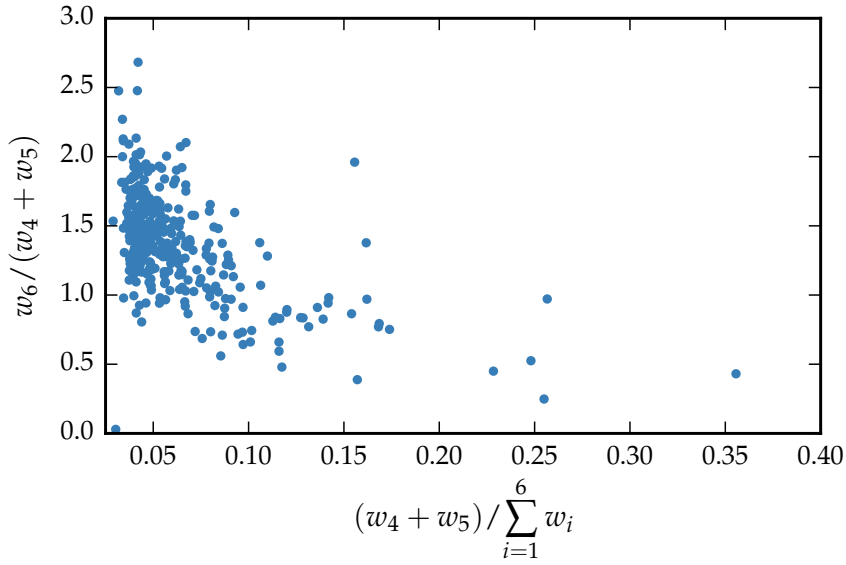Figure 1.15: ICA median weights as a functino of the CIV blueshift.

Figure 1.16: Zhang et al. 2011: Blueshift of [O III] correlates significantly with the EQW of the core. The more the peak of the line is blueshifted, the more the core component decreases dramatically, while the blue wing changes much less. We see this clearly. This is similar to behaviour of C IV? I.e. is there a mapping from this to the C IV space diagram? This would suggests that the mechamism producing the two corerlations is the same. Consistent with the core coming from the canonical extended NLR where the gas is dominate by gravity of the bulge while the wing arises in an outflow. And C IV explained by wind. Suggests intimate connection between BLR and NLR.

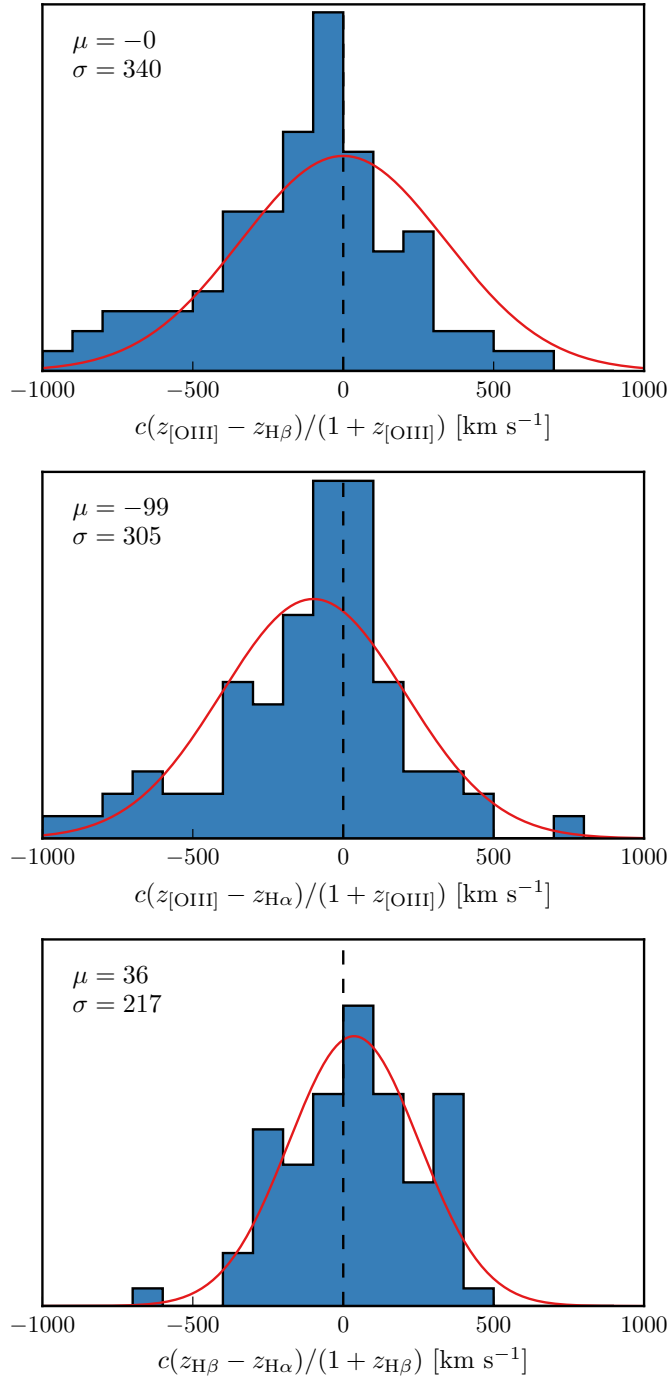Figure 1.17: Redshift comparisons. Lots have been excluded from Ha/Hb so need to look at flags greater than one. What is the big peak? Gaussian fit to the first one has failed. Find out why these plots look different to ones in paper.

from the model with the lowest reduced chi-squared is less than ten per cent.

The models we test are: (1) a single broad Gaussian; (2) two broad Gaussians with identical velocity centroids; (3) two broad Gaussians with different velocity centroids; (4) two broad Gaussians with identical velocity centroids, and additional narrower Gaussians to model the narrow Hα emission, and the narrow components of [N II]λλ6548,6584 and [S II]λλ6717,6731; (5) two broad Gaussians with different velocity centroids, and additional narrower Gaussians. If used, the width and velocity of all narrow components are set to be equal in the fit, and the relative flux ratio of the two [N II] components is fixed at the expected value of 2.96. The number of quasars fit by each model is: model 1 - 10; model 2 - 71; model 3 - 32; model 4 - 51; model 5 - 53. The redshift is then measured at the peak flux of the Hα model, including both the broad and narrow components of Hα if appropriate.

1.5.2 *ICA*

The only sensible way to measure the systemic redshift is using the NIR ICA fit. Hα and Hβ seem to give no systematic offset but large scatter, and they are often asymmetric, so should only use peak. And Hα isn't always available, and have other narrow components need to decompose. O III peak is mostly fine to use, but then there are some objects where the whole line is blueshifted. And critically, at large CIV blueshifts the [O III] emission is often undetected. Can show comparison of NIR ICA redshifts to... Optical ICA? Hewett & Wild?

Should emphasise that most people use [O III] to get the most reliable systemic redshift. While this is fine at low luminosities, at high luminosities this can result in large errors (profile can be dominated by blueshifted component, Fe emission can be improperly subtracted, or [O III] might not be detected at all. Publish ICA components with this paper?

Can also describe what I found trying to get redshifts from broad Hα, Hβ? (Narrow components generally very weak at these luminosities so can't be used.) Generally find no systematic errors but large ($\sim$1000km s^{-1} scatter). Comparing NIR ICA to [O III] for the [O III] with high S/N I find small (few hundred km s^{-1}) scatter.

Should publish [O III] redshifts with this paper for people to use.

1.5.3 *Parameter uncertainties and upper limits*

Describe how uncertainties on best-fitting parameters were calculated.

In 78 quasars, or approximately 25 per cent of or sample, the [O III] is undetected, or detected with very low S/N. In this section we de-

scribe how upper limits on the [O III] equivalent width were calculated. Firstly, the best-fitting model comprising the continuum, Fe II, and Hβ emission is subtracted from the spectra, leaving behind only emission due to [O III]. From this spectra we generate 100 mock spectra, where the flux at each wavelength is randomly drawn from a Normal distribution with a mean equal to the flux convolved with a Gaussian of width $200\,\mathrm{km\,s^{-1}}$ and a width equal to the known error. We then perform an error-weighted linear least-squares regression with an [O III] template derived from a fit to a very high S/N low redshift SDSS composite spectra. The equivalent width of the best-fitting model is recorded for each of the 100 realisations of the spectra. The error in the equivalent width is defined as the root-mean-square of these values.

Calculated uncertainties using Monte Carlo. Uncertainties on v10 are very large, which I think makes sense since the wing Gaussian will be appearing and disappering, giving a large dispersion in v10. Or regardles v10 is just very sensitive to the noise. Maybe I should be using v25 instead?

1.5.4 *Absolute flux calibration of spectra and continuum luminosities*

Relative flux-calibration of the infrared spectra as a function of wavelength has been achieved, to $\simeq 10$ per cent, through observations of appropriate flux standards. The absolute flux levels, however, can be in error by large factors due to variable atmospheric conditions combined with the narrow slit widths. For the majority of the quasars we have, therefore, established the absolute flux scale for each near-infrared spectrum using the same quasar SED-model fitting scheme employed in Paper I. Briefly, the SED-model was fit, with the normalisation and E(B-V) as free varibales, to optical/infrared magnitudes, or SDSS/BOSS spectra (check order I do this.) This allows us to extrapolate from the optical when we do not have photometric data in the near-infrared. The spectra were then normalised to the SED model using a linear error-weighted least-squares regression in the the regions of the spectra covered by the H/K bands. The monochromatic continuum luminosity at 5100Åwas calculated directly from the normalised SED-model. **If this sounds strange can also calculate from fit to normaised spectra. Check if any missing normalisation / monochromatic luminosities.**

1.6 RESULTS FROM ICA FITS

Need to convince the reader that the ICA components approximately correspond to real components. Explain how non-parameteric measures derived form ICA reconstructions.
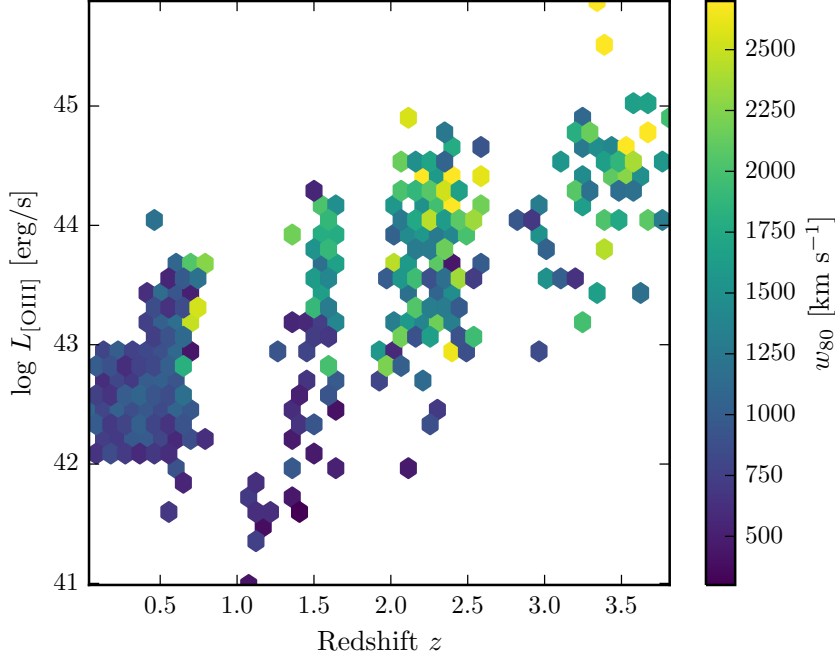
Figure 1.18: The [O III] velocity-width, characterised by w_{80}, as a function the [O III] luminosity and the quasar redshift. The color of each hexagon denotes the mean w_{80} for the obects in that luminosity-redshift bin. We have suplemented our sample with low-z objects from Zakamska and Greene, (2014) and medium ($z \sim 1.5$) redshift objects from Harrison et al., (2016). If I keep this plot make sure its clear which points belong to which sample.

We find there is a decreasing symmetric component at high luminosities. Relates directly to Shen and Ho, (2014). A stable narrow line region is removed by the outflowing material. Shen and Ho, (2014) showed that the strength of the core [O III] component decreases with quasar luminosity and optical Fe II strength faster than the wing component, leading to overall broader and more blueshifted profiles as luminoisty and Fe II strength (or C IV blueshift) increases.

1.7 LUMINOSITY/REDSHIFT-EVOLUTION OF [O III] PROPERTIES

In this section we look for any luminosity/redshift dependent changes in the [O III] line properties. To do this we extend the dynamic range of our samples in terms of both luminosity and redshift by supplementing our sample with quasars presented by Zakamska and Greene, (2014) and Harrison et al., (2016).

The Zakamska and Greene, (2014) objects are a sample of 568 obscured luminous quasars selected from SDSS (Reyes et al., 2008; Yuan, Strauss, and Zakamska, 2016). They are selected to have [O III] luminosities above $10^{8.5} L_\odot$ and have a median redshift $z = 0.397$.

We also include 40 quasars at redshifts $1.1 \leqslant z \leqslant 1.7$) from the KMOS AGN Survey at High redshift (KASHz) with [O III] line measurements.

We also have the same information for ~20 000 SDSS spectra from Mullaney et al., (2013).

In Figure 1.18 we show the [O III] velocity width as a function of the [O III] luminosity and the quasar redshift. The lack of any redshift-evolution between $z = 0$ and $z = 1.5$ was reported by Harrison et al., (2016). Our additional data suggests that this continues to $z \sim 2.5$. On the other hand, at fixed redshift, we see a significant correlation between the [O III] velocity width and the luminosity.

The fact that we don't see many broad lines in the Zakamska and Greene, (2014) objects even at luminosities >43 erg/s could be due to the fact that these are all type II quasars, whereas the sample presented in this paper are all type I. Mullaney et al., (2013) showed that the [O III] lines of type I quasars are typically broader than in type II quasars.

Looking at the [O III] velocity width as a function of luminosity tells us about the physical drivers of the outflows observed in [O III]. The correlation with luminosity suggests that the highest velocity outflows are associated with the most luminous AGN. This has been reported for low-redshift AGN, for both ionized and molecular outflows (e.g. Westmoquette et al. 2012; Veilleux et al. 2013; Arribas et al. 2014; Cicone et al. 2014; Hill & Zakamska 2014).

This suggests that the outflows are driven by radiative forces. On the other hand, Mullaney et al., (2013) find that once the correlation between the [O III] luminosity and the radio luminosity has been taken in to account, the [O III] velocity width is more strongly related to the radio luminosity of the AGN.

1.8 EQUIVALENT WIDTH

In Fig. 1.19 we show the [O III]5008 EW as a function of the quasar bolometric luminosity. Bolometric luminosity is estimated from the monochromatic continuum luminoisty at 5100Åusing the correction factor given by Richards et al., (2006). For comparison, we also show the low-z sample from Shen et al., (2011).

The equivalent width of [O III] has been found to strongly decrease as a function of redshift and/or luminosity (e.g. Brotherton, 1996; Netzer et al., 2004; Sulentic et al., 2004; Baskin and Laor, 2005).

The size of the narrow line region is roughly expected to scale as $L^{0.5}$ (e.g. Netzer et al., 2004). However, for high luminosity quasars with strong [O III] this gives NLR sizes which are unreasonably large (~100 kpc; Netzer et al., 2004).

Netzer et al., (2004) found 1/3 of their high luminosity sample had very weak [O III], whereas quasars with weak [O III] are very rare
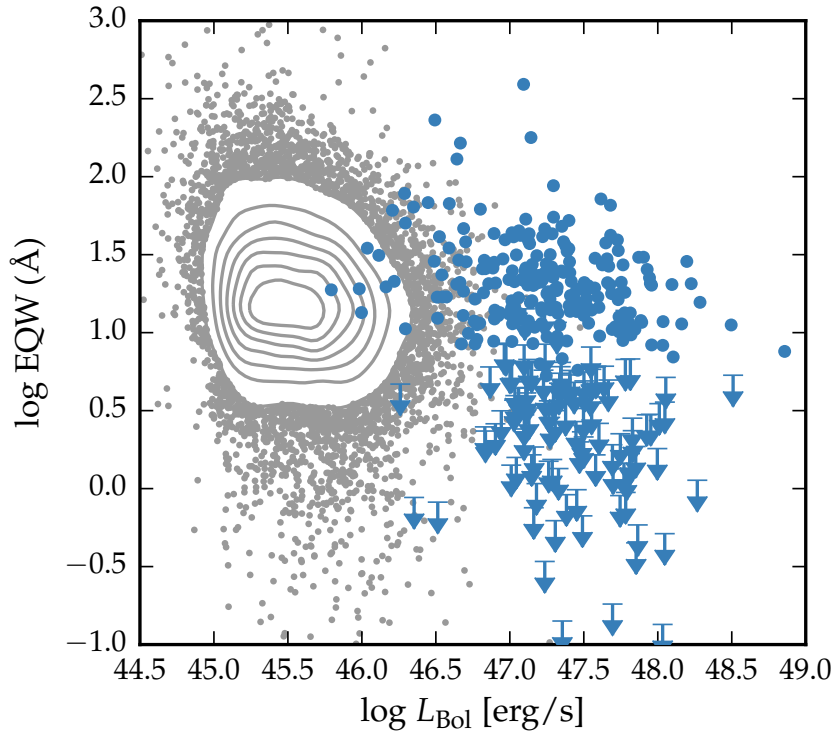
Figure 1.19: The [O III] EW as a function of the quasar bolometric luminosity for the sample presented in this paper (blue circles) and the low-z SDSS sample (grey points and contours). Upper limits are denoted by the downward arrows.
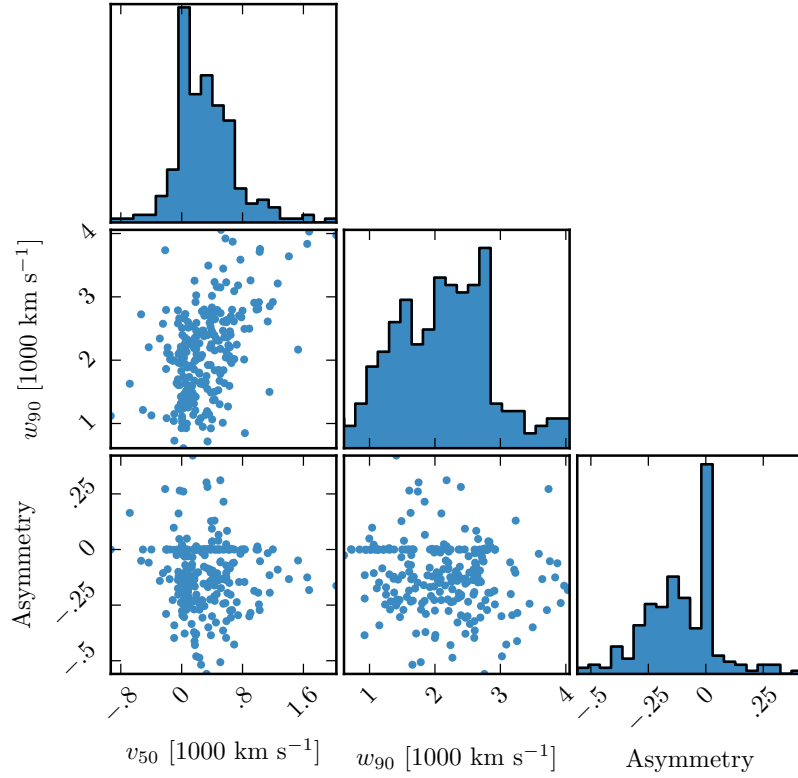
Figure 1.20: The distributions of and correlations between a subset of the non-parameteric measures we made of the best-fitting [O III] models.

for nearby AGN. We find a very similar fraction. Netzer et al., (2004) claim that for the population of strong [O III] emitters there is no reduction of EW with increasing source luminosity. On the other hand, there are many weak or no [O III] emitters at high luminosity that could give the impression that the line EQW decreases with increasing source luminoisity.

1.8.1 *OIII outflows*

Our best-fitting profiles show a strongly blue-asymmetric profile (Fig. 1.20), with a significant fraction of the total emission in a blue wing. The luminous blueshifted broad wing and the exteremely broad profile reveals high-velocity outflowing ionized gas. This can be explained if the far-side of any outflowing gas, that is moving away from the line of sight, is obscured by dust in the host galaxies (e.g. Heckman et al. 1981; Vrtilek 1985). Observations at both low and high redshifts commonly observe this blueshifted component. Our results, and those of other authors, suggest that kpc-scale outflows

in ionized gas are common among the most luminous high-redshift actively accreting SMBHs.

The situation is very different in nearby AGN, where the [O III] velocity width is dominated by the galactic potential and correlates well with the stellar velocity dispersion. HI, CO and absorption line mesaures of the host galaxy rest frame suggest that [O III] usually gives consistent results within 200 km/s (de Robertis 1985; Whittle 1985; Wilson & Heckman 1985; Condon et al. 1985; Stripe 1990; Alloin et al. 1992; Evans et al. 2001).

We see a correlation between the [O III] velocity width and blueshift. As the blueshift of the line increases it gets broader. This is consistent with Shen and Ho, (2014), where the strength of the narrow core is decreasing, leading to a broader and more blueshifted profile.

1.8.2 *[O III] and C IV outflows are linked*

As described in Paper I, we have searched for optical counterparts to our near-infrared spectra. Optical spectra are available for XXX quasars in our catalogue, and cover the broad C IV doublet. As we described in Paper I and Coatman et al., (2016), C IV is often blueshifted, which almost certainly signal the presence of strong outflows, most likely originating in a disc wind. In Paper I we demonstrated that the quasars in our sample cover the full range of C IV blueshifts seen in the SDSS quasar population, which makes our sample unique in that it allows us to study properties of the quasar across the full parameter range.

The C IV velocity centroid measurements are taken directly from paper I. We define the 'location' of the [O III] emission using v_{10}, although the results are the same if v_{20}, v_{50} etc. are used instead.

In Figure 1.21 we show the C IV blueshifts against the [O III] blueshifts. This comparison is done for a sub-sample of 146 objects where we have good measurements of the C IV, [O III], and Hβ (to measure the systemic redshift) profiles. Objects with S/N > 3 are shown as blue filled circles and objects with S/N < 3 as open grey circles. We calculated the median S/N per pixel in the best-fitting model for the [O III]5008 emission.

There is a clear and strong correlation. Similar correlations have been tentatively found in lower redshift quasars and AGN (Zamanov et al., 2002).

The blueshifting of C IV is known to correlate with luminosity (Richards et al., 2011). In [O III], the blueshifted wing becomes relatively more prominent as the luminosity of the quasar increases (Shen and Ho, 2014). Therefore, it is plausible that the correlation between the C IV and [O III] blueshifts is a secondary effect that is driven by the correlation of each with the luminosity. In Figure **??** we color the data
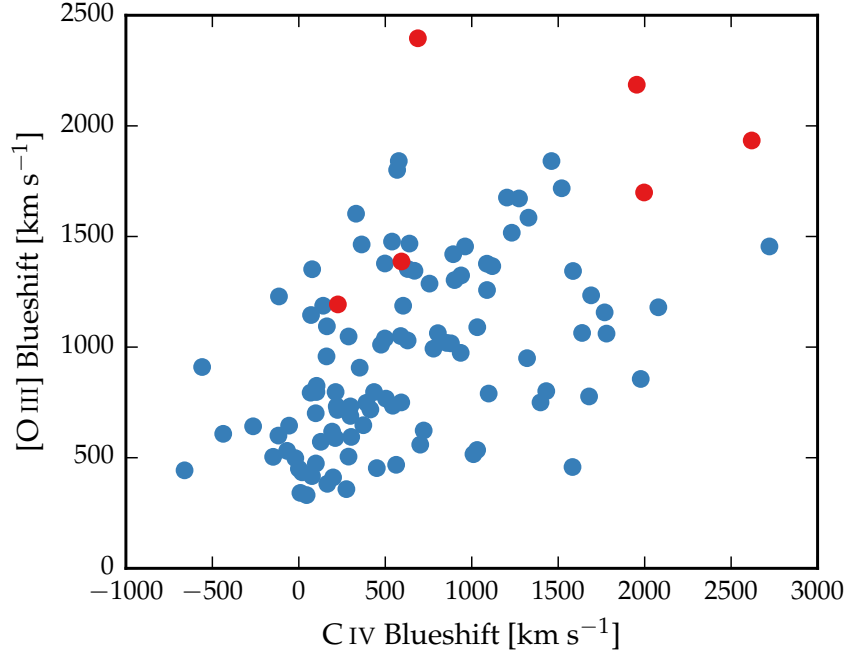
Figure 1.21: The relation between the blueshifts of C IV and [O III]. Equivalent to Fig 8. We use the Hβ peak in this figure, which I think is responsible for some of the trend. However, we do see a correlation (albeit noisier) using the NIR ICA redshifts. Not a sensible to use the [O III] redshifts, since these become much more unreliable at the high C IV blueshift end (when [O III] is weaker: figure 7. Note that we are using v_{10} for the [O III] position and v_{50} for the C IV position. We can't use v_{50} for [O III] because sometimes we are using a single Gaussian, especially if the [O III] is weaker and we miss the broad component. Need to remake this plot / don't use at all because I don't believe some of the Gaussian fits to [O III], especially at high C IV blueshifts when [O III] is weak and Fe II is strong.) Only objects where fit with two components.
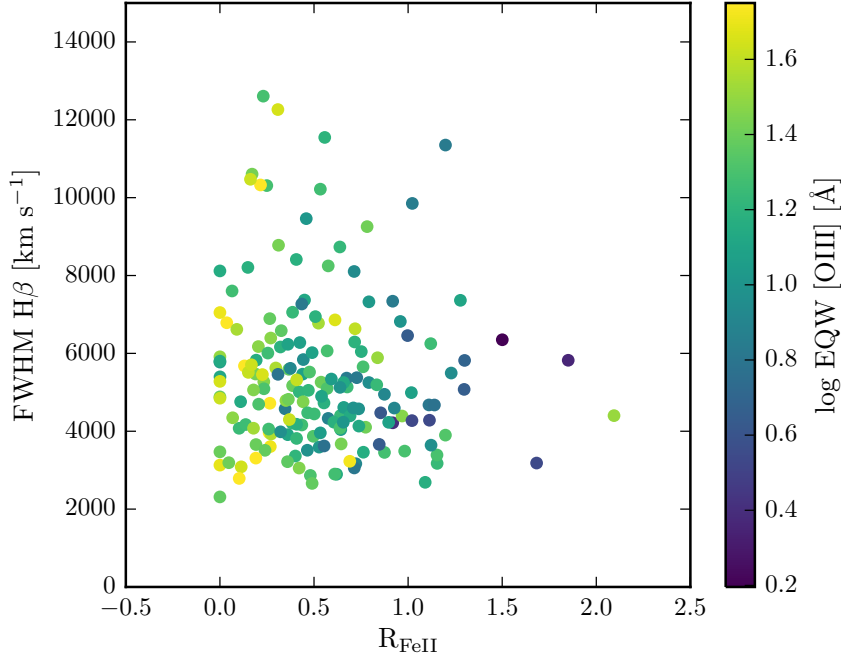
Figure 1.22: The [O III] EQW as a function of the Hβ FWHM and the optical Fe II strength (EQW Fe II/ EQW Hβ).

points by the luminosity, and no luminosity-dependent trends are apparent. We find that both the [O III] and C IV blueshifts are correlated with the luminosity, but that these correlations are much weaker than the correlation between the [O III] and C IV blueshifts.

1.9 EIGENVECTOR ONE CORRELATIONS

Because of this diversity, it is the dominant variable in the set of correlations making up EV1, which is believed to be linked to certain fundamental parameters of the accretion process. In Figure 1.22 we show the [O III] EQW as a function of the Hβ FWHM and the optical Fe II strength. The optical Fe II strength is defined as the ratio of the Fe II and Hβ EQW, where the Fe II EQW is measured between 4434 and 4684Å. These parameters form part of 'eigenvector 1' (EV1), the first eigenvector in a principal component analysis which originated from the work of Boroson and Green, (1992). In our sample, these parameters follow very similar correlations to what is observed at low-z (e.g. Shen and Ho, 2014). In particular, the anti-correlation between the [O III] and Fe II EQWs.

Same as Shen, (2016), we confirm that the EV1 correlations hold at high luminosities/redshifts. See also Sulentic et al. 2004, 2006; Runnoe et al. 2013. Make sure it's clear that Shen, (2016) quasars make up a significant chunk of our sample.
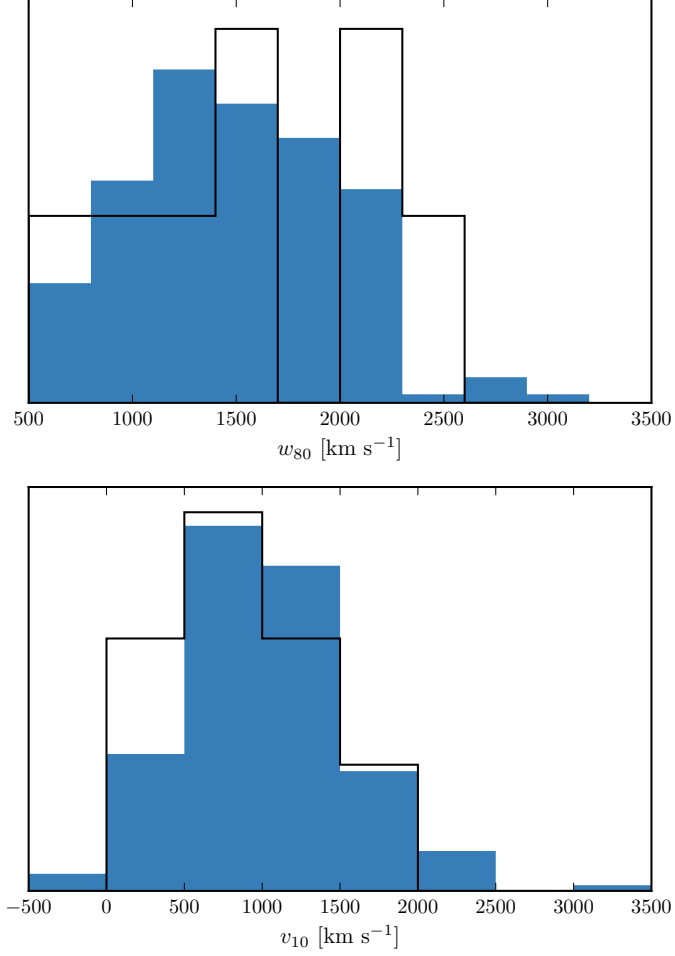
Figure 1.23: The distribution of w_{80} and v_{10} for the 19 BALs are compared to the distribution for the non-BALs. These look rubbish. Cumulative distributions instead? Try doing gaussian kernel density estimator

1.10 MAPPING EV1 TO CIV BLUESHIFT AND EQW

1.11 SIGNAL TO NOISE TESTS

1.12 BROAD ABSORPTION LINE QUASARS

19 quasars in our catalogue are classified as broad absorption line (BAL) quasars, using the either the SDSS classification flags or the Allen et al., (2011) catalogue. We find that the BAL quasars have typically broader [O III] than the rest of the sample. Note that in the Zakamska et al., (2016) sample of very red quasars, the incidence of BALs is very high, and these objects have extremely broad [O III] profiles. A two-sided Kolmogorov-Smirnov statistic on the w_{80} distributions returned a p-value of 0.10. What does this mean? Try with

different parameters? Histograms look rubbish so maybe just give the numbers.

1.13 DISCUSSION

1.13.1 *Type II quasars*

Implications of our findings on searches for high-redshift type 2 quasars. It could be that type II quasars exist. If you look at CIV/MgII the narrow line components are very weak. So the contribution from the narrow line region is very weak in luminous quasars, and you just won't see it even if the broad line region is obscured. Findings in this paper seem to suggest that the startic narrow line region is very weak in luminous quasars.